Microneedle-array patches loaded with hypoxia-sensitive vesicles provide fast glucose-responsive insulin delivery

Jicheng Yu[a,b], Yuqi Zhang[a,b], Yanqi Ye[a,b], Rocco DiSanto[a,b], Wujin Sun[a,b], Davis Ranson[a], Frances S. Ligler[a], John B. Buse[c], and Zhen Gu[a,b,c,1]

[a]Joint Department of Biomedical Engineering, University of North Carolina at Chapel Hill and North Carolina State University, Raleigh, NC 27695; [b]Molecular Pharmaceutics Division and Center for Nanotechnology in Drug Delivery, Eshelman School of Pharmacy, University of North Carolina at Chapel Hill, Chapel Hill, NC 27599; and [c]Department of Medicine, University of North Carolina School of Medicine, Chapel Hill, NC 27599

Edited by Dean Ho, University of California, Los Angeles, CA, and accepted by the Editorial Board May 19, 2015 (received for review March 17, 2015)

A glucose-responsive "closed-loop" insulin delivery system mimicking the function of pancreatic cells has tremendous potential to improve quality of life and health in diabetics. Here, we report a novel glucose-responsive insulin delivery device using a painless microneedle-array patch ("smart insulin patch") containing glucose-responsive vesicles (GRVs; with an average diameter of 118 nm), which are loaded with insulin and glucose oxidase (GO_x) enzyme. The GRVs are self-assembled from hypoxia-sensitive hyaluronic acid (HS-HA) conjugated with 2-nitroimidazole (NI), a hydrophobic component that can be converted to hydrophilic 2-aminoimidazoles through bioreduction under hypoxic conditions. The local hypoxic microenvironment caused by the enzymatic oxidation of glucose in the hyperglycemic state promotes the reduction of HS-HA, which rapidly triggers the dissociation of vesicles and subsequent release of insulin. The smart insulin patch effectively regulated the blood glucose in a mouse model of chemically induced type 1 diabetes. The described work is the first demonstration, to our knowledge, of a synthetic glucose-responsive device using a hypoxia trigger for regulation of insulin release. The faster responsiveness of this approach holds promise in avoiding hyperglycemia and hypoglycemia if translated for human therapy.

diabetes | drug delivery | glucose-responsive | hypoxia-sensitive | microneedle

Diabetes mellitus is a group of metabolic diseases characterized by failure of blood glucose level regulation mechanisms (1, 2). As of 2014, 387 million people suffered from diabetes worldwide, and the number is estimated to be 592 million by 2035 (3, 4). The traditional care for people with diabetes often requires monitoring of blood glucose and insulin injections to maintain normoglycemia (5). However, such self-administration is associated with pain and often inadequate glucose control (6–8). Poor glucose control accounts for a high risk for complications of diabetes, including limb amputation, blindness, and kidney failure. Additionally, hypoglycemia can result in behavioral and cognitive disturbance, seizure, loss of consciousness, coma, brain damage, or death (9).

An artificial pancreas-like, closed-loop, glucose-responsive insulin delivery system that is able to "secrete" insulin in response to elevated blood glucose would provide a desirable way of regulating glycemia with minimal patient effort and potential improvements in glycemia and quality of life (6, 7, 10). Current closed-loop systems combine a glucose-monitoring module and a sensor-triggered insulin releasing module (6, 7). There are closed-loop electronic/mechanical devices that use a continuous glucose-monitoring sensor calibrated by the patient and an external insulin infusion pump (8). However, challenges associated with such devices, such as guaranteeing accurate signal feedback and preventing biofouling, still persist. A chemical approach using an insulin-loaded matrix with glucose-sensing elements and a relevant actuator could avoid those limitations and may prove more effective for closed-loop insulin release. The matrix can undergo structural transformations (i.e., shrink, swell, dissociate) regulated by glucose concentration changes, leading to glucose-stimulated insulin release (11–14). The typical glucose-sensing moieties include phenylboronic acid (PBA), glucose-binding protein (GBP), and glucose oxidase (GO_x) (12–20). Despite these available sensing chemistries, the majority of existing synthetic closed-loop systems have only been studied in vitro, with relatively few showing applicability in vivo due to specific challenges for each glucose-sensing strategy. For example, PBA and its derivatives are known for their reversible interaction with polyol molecules, such as glucose (21), but an efficient interaction between glucose and PBA, with a subsequent structural change in the matrix, usually requires a more basic pH than is present in the physiological environment. The safety and toxicity of PBA conjugates also remain to be established. Con A is the most commonly used GBP for insulin delivery, generally based on its multiple binding sites and competitive interaction with glucose and dextran matrix (22). However, the verified in vivo toxicity and instability of Con A limit its clinical applications (23). GO_x is an enzyme that can convert glucose to gluconic acid in the presence of oxygen (10):

$$\text{Glucose} + O_2 + H_2O \xrightarrow{GO_X} \text{Gluconic Acid} + H_2O_2.$$

Glucose-responsive systems using GO_x are always integrated with pH-sensitive materials, which are either protonated or degraded with a local decrease of pH, promoted by increasing glucose

Significance

For exploiting synthetic glucose-responsive insulin delivery systems, challenges remain to demonstrate a strategy that would combine (*i*) fast responsiveness, (*ii*) ease of administration, and (*iii*) excellent biocompatibility. We have developed a novel glucose-responsive insulin delivery device using a painless microneedle-array patch containing hypoxia-sensitive hyaluronic acid-based vesicles. The vesicles quickly dissociate and release encapsulated insulin under the local hypoxic environment, caused by the enzymatic oxidation of glucose in the hyperglycemic state. This "smart insulin patch" with a new enzyme-based glucose-responsive mechanism can regulate the blood glucose of type 1 diabetic mice to achieve normal levels, with faster responsiveness compared with the commonly used pH-sensitive formulations, and can avoid the risk of hypoglycemia.

Author contributions: J.Y. and Z.G. designed research; J.Y., Y.Z., Y.Y., R.D., W.S., and D.R. performed research; J.Y., Y.Z., Y.Y., F.S.L., J.B.B., and Z.G. analyzed data; and J.Y., Y.Z., Y.Y., F.S.L., J.B.B., and Z.G. wrote the paper.

The authors declare no conflict of interest.

This article is a PNAS Direct Submission. D.H. is a Guest Editor invited by the Editorial Board.

[1]To whom correspondence should be addressed. Email: zgu@email.unc.edu.

This article contains supporting information online at www.pnas.org/lookup/suppl/doi:10.1073/pnas.1505405112/-/DCSupplemental.

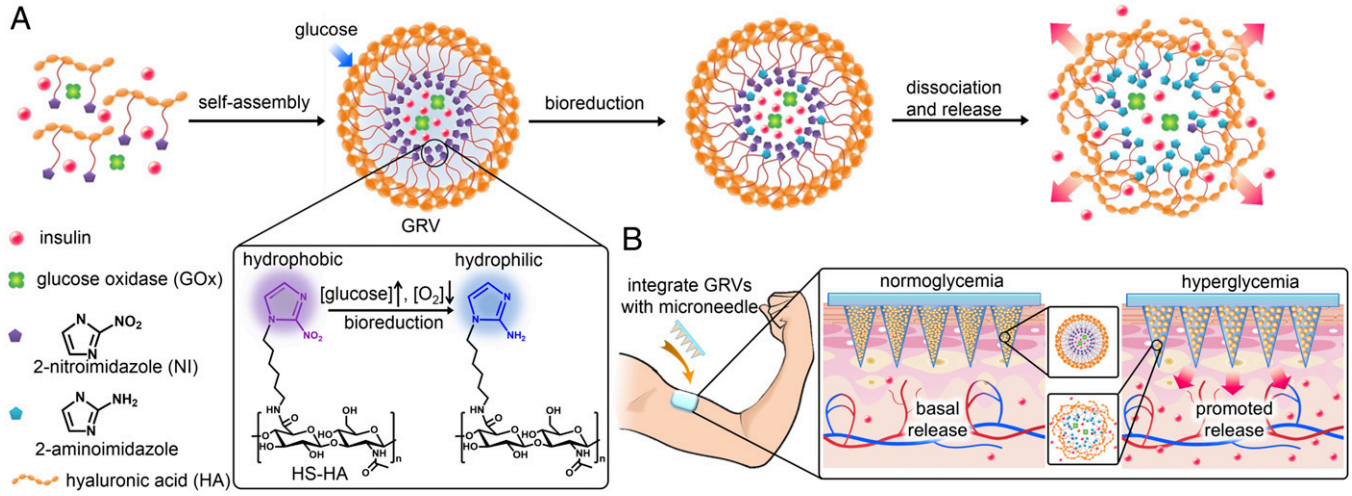

Fig. 1. Schematic of the glucose-responsive insulin delivery system using hypoxia-sensitive vesicle-loading MN-array patches. (*A*) Formation and mechanism of GRVs composed of HS-HA. (*B*) Schematic of the GRV-containing MN-array patch (smart insulin patch) for in vivo insulin delivery triggered by a hyperglycemic state to release more insulin.

concentration. However, such pH decrease-dependent methods are often compromised by slow responsiveness, especially in a buffered physiological environment (8). Taken together, challenges remain to demonstrate a method that would combine (*i*) fast responsiveness with pharmacokinetics similar to normal pancreatic activity, (*ii*) ease of administration, and (*iii*) biocompatibility without long-term side effects (3).

Here, we report a novel glucose-responsive insulin delivery device based on microneedle (MN)-array patches integrated with hypoxia-sensitive hyaluronic acid (HS-HA) vesicles containing insulin and GO_x. Instead of using enzymatically induced pH changes (3, 8), for the first time to our knowledge, we have taken advantage of the local generation of hypoxia due to the consumption of oxygen in the enzymatic reaction as a trigger for rapid insulin release in response to hyperglycemia. To achieve hypoxia-responsive transduction, 2-nitroimidazole (NI), a hydrophobic component that has often been applied in cancer imaging due to its high sensitivity to the hypoxic condition in tumor sites, was used (24, 25). NI can be converted to hydrophilic 2-aminoimidazoles under a hypoxic environment via a single-electron reduction catalyzed by a series of nitroreductases coupled to bioreducing agents, such as NADPH, a plentiful coenzyme in tissues (24–27). We conjugated amine-functionalized NI with HA (molecular mass of 300 kDa), which is well known to have excellent biocompatibility and biodegradability (28–30). As shown in Fig. 1*A*, through self-assembly, the amphiphilic HS-HA can readily form nanoscale glucose-responsive vesicles (GRVs) encapsulating both recombinant human insulin and GO_x in an aqueous solution. In the presence of a high blood glucose level, the dissolved oxygen can be rapidly consumed due to the glucose oxidation catalyzed by GO_x (3, 10), which produced a local hypoxic environment. NI groups on the HS-HA were then reduced into hydrophilic 2-aminoimidazoles under bioreductive conditions, which resulted in the dissociation of GRVs and subsequent release of insulin.

To realize ease of administration, we further loaded the GRVs into a MN-array patch for painless (31–34) insulin delivery (Fig. 1*B*). The matrix of MNs was made from cross-linked HA to improve the stiffness of MNs and restrict the loss of GRVs from needles. With transcutaneous administration, the GRVs loaded in MNs disassembled when exposed to high interstitial fluid glucose in vascular and lymph capillary networks (35), thereby promoting the release of insulin, which was then taken up quickly through the regional lymph and capillary vessels (36). We demonstrated that this "smart insulin patch" with a novel glucose-responsive mechanism displayed rapid responsiveness for glucose regulation and reliable avoidance of hypoglycemia in a mouse model of type 1 diabetes.

Results

Synthesis and Characterization of GRVs. GRVs were formed by self-assembly of HS-HA, encapsulating recombinant human insulin and GO_x in the core. The HS-HA was obtained via the formation of an amide bond with amine-functionalized NI in three steps (Fig. S1). The incorporation of hydrophobic NI groups renders the derived HA amphiphilic, enabling the formation of GRVs in the aqueous solution (37, 38). Moreover, NI provides an hypoxia-sensitive element, which is expected to be bioreduced under hypoxic conditions (24, 27). The reduced product with amine groups is water-soluble, leading to disassembly of GRVs. As presented in the transmission electron microscopy (TEM) image (Fig. 2*A*), the resulting GRVs had a spherical shape with a monodisperse size. The average diameter of GRVs was determined as 118 nm by dynamic light scattering (DLS) (Fig. 2*B*), which is consistent with observation by TEM. The zeta-potential of GRVs was measured as -34.7 ± 0.4 mV due to the residual carboxyl of HA. The fluorescence image of GRVs with FITC-labeled insulin further verified successful encapsulation of insulin (Fig. 2*D*). The insulin loading capacity of GRVs was determined as 8.7% (wt/wt). Importantly, the obtained GRVs were highly stable, and no significant precipitation was observed at 4 °C for 1 mo.

In Vitro Glucose-Responsive Insulin Release of GRVs. To examine the glucose-responsive disassembly of GRVs, vesicles were incubated with PBS buffer [137 mM NaCl, 2.7 mM KCl, 10 mM Na_2HPO_4, 2 mM KH_2PO_4 (pH 7.4)] containing different concentrations of glucose, including a typical hyperglycemic level (400 mg/dL), a normoglycemic level (100 mg/dL), and a control level (0 mg/dL). The oxygen consumption, caused by the oxidation of glucose catalyzed by GO_x, was measured using an oxygen-sensitive phosphorescent molecular probe (39, 40). As presented in Fig. 2*F*, the sample exposed to the hyperglycemic solution had a lower oxygen concentration compared with the other two control samples. Of note, equilibrium was achieved in 10 min, suggesting that the oxygen consumption rate reached equilibrium with the dissolution rate at this time. The recorded pH value of incubating solutions with 400 mg/dL glucose solution decreased steadily over time (Fig. S2), further substantiating the conversion of glucose to gluconic acid catalyzed by GO_x. In this hypoxic environment, the nitro groups of the HS-HA were effectively reduced by electrons from NADPH catalyzed by the reductase. The residual concentration of NI was monitored in real time by

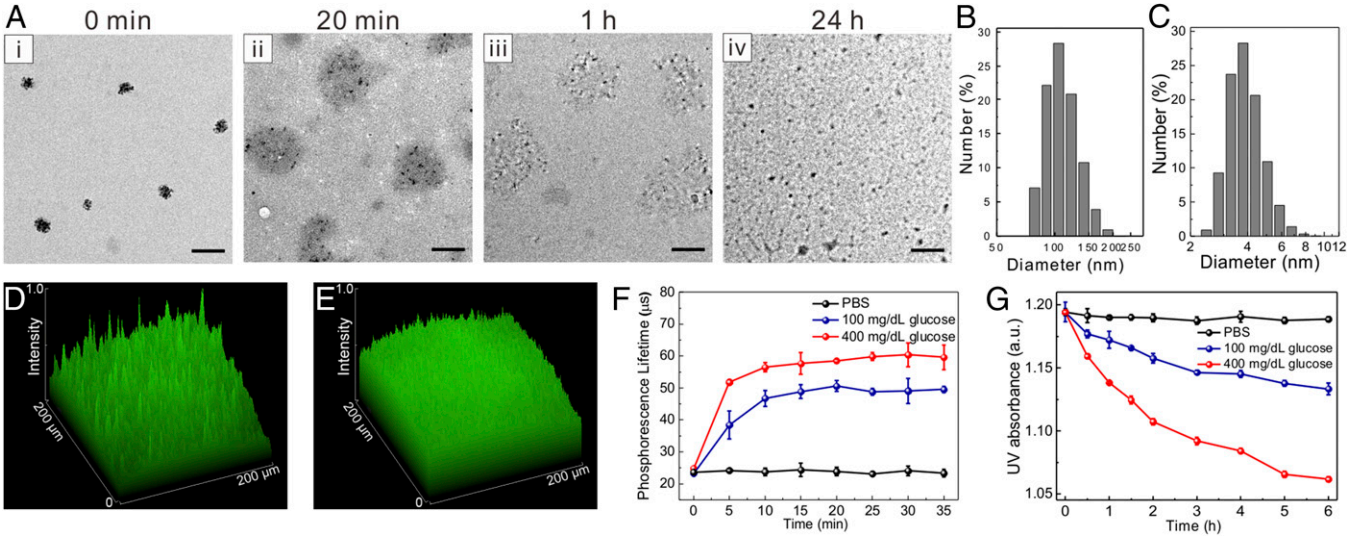

Fig. 2. Characterization of GRVs. (*A*) TEM images of GRV-encapsulated insulin and enzyme (*i*) preincubation or postincubation with 400 mg/dL glucose for (*ii*) 20 min, (*iii*) 1 h, and (*iv*) 24 h. (Scale bars: 200 nm.) Size distribution of GRVs preincubation (*B*) and postincubation (*C*) with 400 mg/dL glucose for 24 h. Fluorescence 2.5D images of FITC-insulin–loaded GRV solution preincubation (*D*) and postincubation (*E*) in 400 mg/dL glucose solution for 1 h at 37 °C. (*F*) Phosphorescence lifetime profile over time for the GRVs incubated with different glucose concentration solutions containing an oxygen concentration molecule probe. (*G*) Monitoring of UV absorbance intensity of GRVs at A_{330} over time in different glucose concentrations at 37 °C. Error bars indicate SD ($n = 3$). a.u., arbitrary unit.

measuring the UV-visible (UV-Vis) absorbance intensity of the characteristic peak of NI at A_{330} (41). As shown in Fig. 2*G*, the corresponding absorbance intensity of GRVs incubated with 400 mg/dL glucose solution gradually decreased over time, suggesting the replacement of hydrophobic NI groups with amine groups. In sharp contrast, a much slower decline of absorbance intensity was observed in the samples associated with 100 mg/dL glucose solution, and no decrease was observed in the control sample without glucose. Furthermore, the corresponding evolution of conformation and size changes were clearly observed through TEM imaging and DLS (Fig. 2 *A* and *C*). To validate the release of insulin from the disassembled GRVs further, insulin conjugated with FITC was encapsulated into GRVs. As demonstrated in Fig. 2*E*, the fluorescence signal was more homogeneously distributed after exposure of the GRV suspension to glucose for 1 h, while the original GRV suspension showed a large amount of cluster signal, verifying the release of FITC-insulin.

A remarkably rapid insulin release profile was achieved from the sample with a typical hyperglycemic level of 400 mg/dL glucose due to the dissociation of GRVs, whereas only a small amount of insulin was released from the GRVs in PBS solution with none or a relatively normal level of 100 mg/dL glucose (Fig. 3*A*). To validate if the insulin release speed directly corresponds to the reduction of NI groups as a result of oxygen level rather than decreased pH level, the insulin release kinetics in pH 4.0 solution were investigated. The result showed that there was insignificant insulin release of the sample incubated in a pH 4.0 solution, confirming the GRVs were stable under an acidic condition (Fig. S3). In addition, an alterable kinetic release profile of insulin was observed by varying glucose concentration (Fig. 3*B*). A maximum of a 6.6-fold difference in insulin release rate was achieved in 20 min when the glucose concentration was changed from 100 to 400 mg/dL. In contrast, GRVs containing one-half the amount of GO_x showed a slower release rate due to a relatively slower oxygen consumption rate, suggesting that the insulin release rate can be tuned by varying the encapsulation dose of enzyme. Moreover, the insulin release profile of GRVs presented a pulsatile pattern when alternatively exposed between a normal and hyperglycemic state every 20 min for several cycles (Fig. 3*C*). Importantly, the GRVs responded to changes in glucose concentrations rapidly compared with existing synthetic glucose-responsive systems (3, 8). For example, the hypoxia-sensitive GRVs displayed a significantly faster response rate to hyperglycemic levels compared with pH-sensitive–based glucose-responsive formulations previously reported in parallel (19) with the same amount of enzymes (Fig. S4). This finding can be attributed to the faster attainment of the "structural transformation point" for dissociation of the formulation triggered by the local hypoxic microenvironment than by the local acidic environment. Collectively, the results discussed above substantiated that the disassembly of GRVs and the release of insulin underwent a glucose-mediated and hypoxia-dependent process. Additionally, the CD spectrum showed that the secondary conformational structure of released insulin from GRVs (0.1 mg/mL) did not change compared to that of the native insulin (Fig. 3*D*).

Fabrication and Characterization of GRV-Loaded MN-Array Patch. To achieve convenient administration, we next fabricated an MN-array (32, 34, 42) patch containing GRVs as a painless and disposable modality (32) for administering insulin. Briefly, the GRVs were first loaded in tips of a silicone mold for MNs by centrifugation, followed by drop-wise addition of a solution containing methacrylated HA, the cross-linker *N*,*N*'-methylenebisacrylamide, and a photoinitiator (Fig. 4*A*). Under UV irradiation, the HA matrix was photo–cross-linked to enhance the stiffness of MNs and entrap the GRVs in the needles. The resulting MNs were arranged in an 11 × 11 array with an area of 6 × 6 mm and backed for stability during handling using medical tape (Fig. 4*B*). Each needle was conical, with a base radius of 150 μm, a height of 600 μm, and a tip radius of ∼10 μm (Fig. 4*C*). Fig. 4*D* shows the fluorescence image of a representative MN that contains FITC-insulin–loaded GRVs, indicating that GRVs were evenly distributed inside the needle tips. Measurement of mechanical strength using a tensile compression machine indicated a failure force for cross-linked MNs of 0.06 N per needle, compared with only 0.02 N per needle for non–cross-linked MNs (Fig. 4*E*). The stiffness of cross-linked MNs provided sufficient strength to facilitate skin insertion without breaking (42).

To investigate whether GRVs encapsulated in the MN maintained their glucose-responsive capability after MN fabrication, the tips of the needles containing GRVs were immersed into PBS buffer containing different concentrations of glucose. As shown in Fig. S5, there was negligible difference between GRVs in the MNs and GRVs free in suspension (Fig. 3*A*).

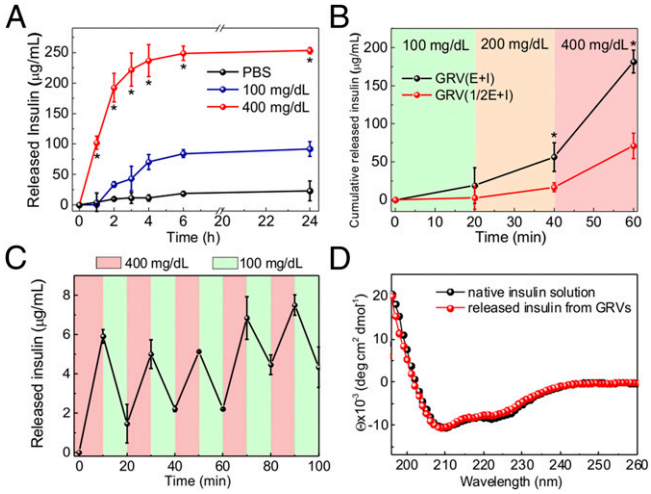

Fig. 3. In vitro glucose-responsive release of insulin from GRVs. (*A*) In vitro accumulated insulin release from the GRVs in several glucose concentrations at 37 °C. *$P < 0.05$ for GRVs in 400 mg/dL glucose solution compared with GRVs in 100 or 0 mg/dL glucose solution. (*B*) Self-regulated profiles of the GRVs and GRVs containing one-half the amount of GO_x present the rate of insulin release as a function of glucose concentration. *$P < 0.05$ for GRV(E + I) compared with GRV (1/2E + I). (*C*) Pulsatile release profile of GRVs presents the rate of insulin release as a function of glucose concentration (100 mg/dL and 400 mg/dL). (*D*) CD spectra of native insulin solution and insulin released from the GRVs incubated with 400 mg/dL glucose. Deg, degree. Error bars indicate SD ($n = 3$).

In Vivo Studies of the MNs for Type 1 Diabetes Treatment. To assess the in vivo efficacy of the MN-array patches for diabetes treatment, the streptozotocin-induced type 1 diabetic mice were grouped and transcutaneously exposed to different samples (Fig. 5*A*, *Top Left*), including the blank MNs containing only cross-linked HA, MNs loaded with human recombinant insulin, MNs loaded with GRVs containing both insulin and enzyme [GRV(E + I)], MNs loaded with GRVs containing insulin and one-half dose of enzyme [GRV(1/2E + I)], or MNs loaded with GRVs containing insulin only [GRV(I)]. The insulin dose applied for each mouse was 10 mg/kg. The MN-array patch penetrated the dorsum skin of the mouse effectively, as evidenced by the trypan blue staining (Fig. 5*A*, *Top Right*) and H&E staining (Fig. 5*A*, *Bottom*). The microchannels on the skin created by the MN-array patch rapidly recovered within 6 h postadministration (Fig. S6). The blood glucose of treated mice in each group was monitored over time. As shown in Fig. 5*B*, the blood glucose in mice treated with GRV(E + I)-loaded MNs quickly declined to nearly 200 mg/dL within 0.5 h and maintained a normoglycemic state (<200 mg/dL) for up to 4 h before gradually increasing. We attributed this fast response rate to the fast generation of the local hypoxic microenvironment that quickly activated the dissociation of GRVs under a bioreductive condition; the relatively low diffusion rate of oxygen in vivo compared with hydrogen ions may facilitate this process further (43–45). When the enzyme dose in the MNs was reduced from 1 to 0.5 mg/kg, the blood glucose levels decreased to around 350 mg/dL within 0.5 h, and steadily increased afterward. In the absence of the enzyme, the glucose levels did not show a noticeable decline, suggesting that the GRVs were highly stable in vivo. Correspondingly, mice administered GRV(E + I)-loaded MNs presented a consistently higher plasma insulin concentration for at least 24 h than those mice treated with GRV(1/2E + I)- and GRV(I)-loaded MNs, as quantified by ELISA (Fig. 5*C*). The SEM image of GRV(E + I)-loaded MNs inserted into skin showed collapse with shortened tips after use (Fig. 5*D*), further confirming that the loaded GRVs disassembled under a hypoxic condition.

Next, a glucose tolerance test was conducted at 1 h after administration of the MNs. The control healthy mice exhibited a quick increase in blood glucose level upon an i.p. glucose injection, followed by a gradual decrease to normoglycemia (Fig. 5*E*). The diabetic mice treated with GRV(E + I)-loaded MNs showed a delayed increase in blood glucose after glucose injection, and then a rapid decline to a normal state within 30 min. However, the glucose of the mice administered insulin-loaded MNs did not decline in 120 min. The area under the curve was calculated between 0 and 120 min to measure the MN responsiveness. As shown, GRV(E + I)-loaded MNs had significantly faster responsivity toward the glucose challenge (Fig. 5*F*).

To assess the in vivo glucose control capability of MN further, the series administration with MNs was performed. The glucose level of mice treated with GRV(E + I)-loaded MNs (dose of 5 mg/kg insulin for each mouse) quickly decreased to around 200 mg/dL within 1 h (Fig. 5*G*). However, glucose did not further decrease to a hypoglycemic level upon application of another dose of GRV(E + I)-loaded MNs (dose 5 mg/kg insulin for each mouse) and maintained a normoglycemic concentration around 200 mg/dL for another 3 h. In contrast, the mice administered GRV(I)-loaded MNs (dose of 5 mg/kg insulin for each mouse) or those mice without additional administration showed a rapid increase in glucose to a hyperglycemic state in 3 h. Insulin-loaded MNs were subsequently administered to another group of mice, and their blood glucose continued to decrease, leading to a risk of hypoglycemia. The study on the healthy mice further indicated there is little insulin leak in GRV-loaded MNs and the risk of hypoglycemia is reduced compared with the insulin-loaded MNs (Fig. 5*H*). The corresponding hypoglycemia index (defined as the fall in glucose from the initial reading to the nadir divided by the time over which this fall was reached) was calculated to measure quantitatively the extent to which insulin elicited hypoglycemia. GRV-loaded MNs showed a remarkably reduced hypoglycemic index compared with insulin-loaded MNs when administered in a normoglycemic state (Fig. 5*I*). Moreover, regarding biocompatibility of the device, HA is found throughout the human body and the bare GRVs did not show significant toxicity at various concentrations studied (Fig. S7). Additionally, there was no significant inflammation observed in the region 2 d postadministration of GRV(E + I)-loaded MNs (Fig. S8).

Discussion

Current GO_x-based glucose-responsive insulin delivery systems mainly use matrices consisting of pH-sensitive materials, which release insulin by either protonation or degradation due to

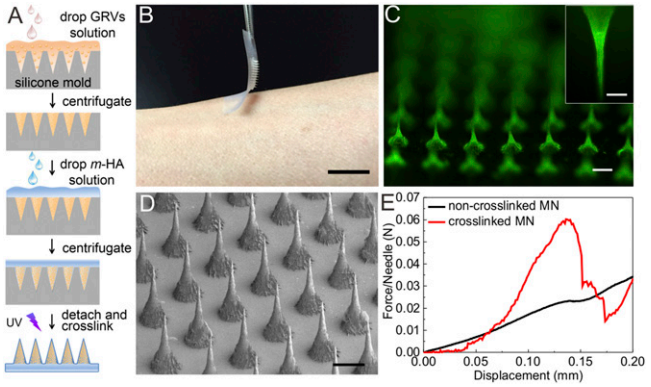

Fig. 4. Characterization of GRV-loaded MN-array patches. (*A*) Schematic of the fabrication process of GRV-loaded MN-array patches from a silicone mold. (*B*) Photograph of the smart insulin patch with an MN array. (Scale bar: 1 cm.) (*C*) Fluorescence microscopy image of MN-loaded GRVs with FITC-labeled insulin. (*Inset*) Zoomed-in image of MN. (Scale bars: 200 μm.) (*D*) SEM image of MN array. (Scale bar: 200 μm.) (*E*) Mechanical behaviors of the non–cross-linked and cross-linked GRV-loaded MNs.

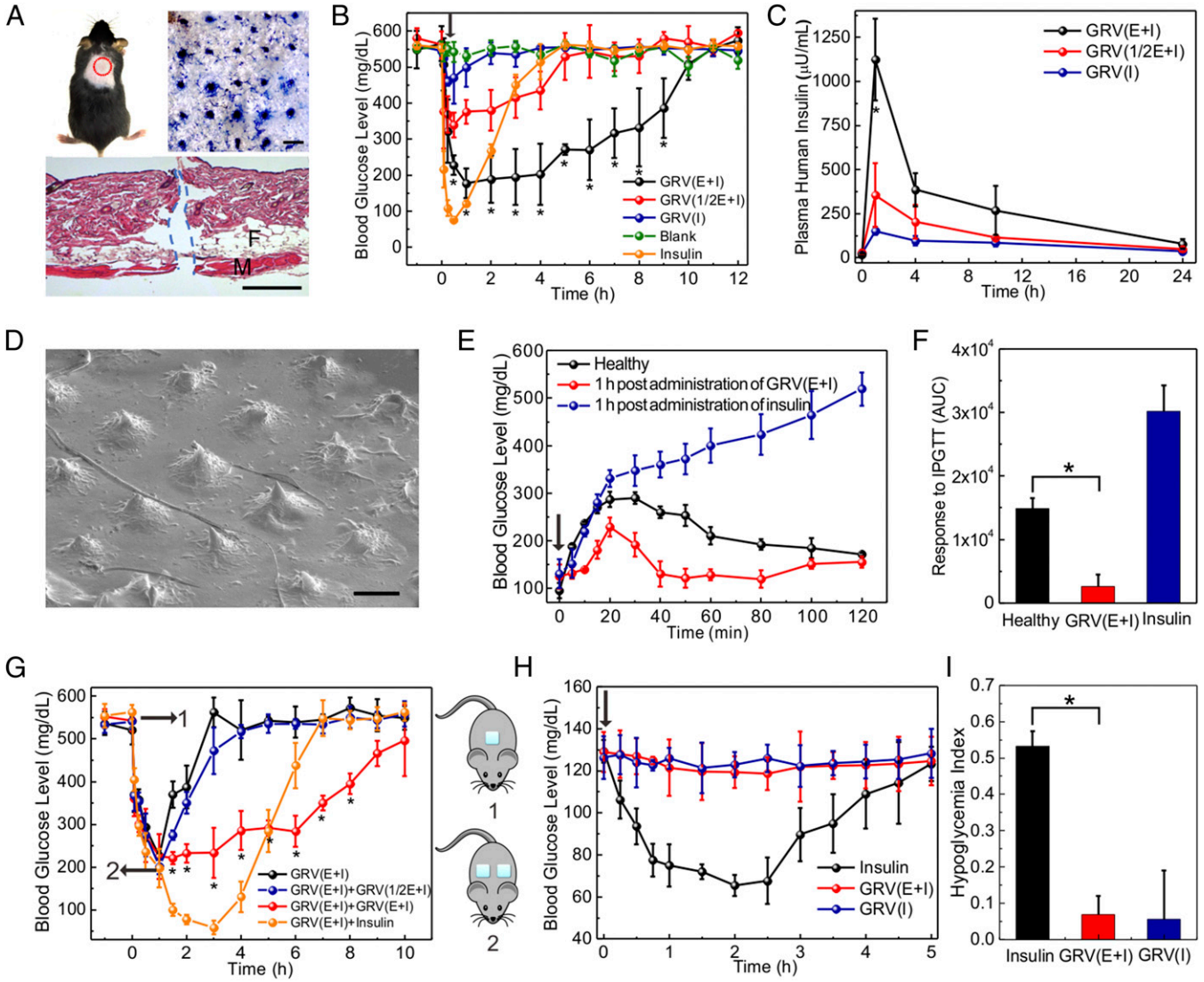

Fig. 5. In vivo studies of the MN-array patches for type 1 diabetes treatment. (*A*) Mouse dorsum and relevant skin (the area within the red dashed line) transcutaneously treated with an MN-array patch (*Top Left*), with the image of the trypan blue staining showing MN-array patch penetration of mouse skin (*Top Right*). (Scale bar: 500 μm.) (*Bottom*) H&E-stained section of mouse skin penetrated by one MN-array patch. The skin muscle and fat tissue regions are indicated by M and F, respectively. The region where MN-array patch insertion took place is indicated by the blue dashed line. (Scale bar: 100 μm.) In vivo studies of the MN-array patches for type 1 diabetes treatment: blood glucose levels (*B*) and plasma human insulin concentrations (*C*) in streptozotocin (STZ)-induced diabetic mice after treatment with blank MNs containing only cross-linked HA, MNs loaded with human recombinant insulin, MNs loaded with GRV(E + I), MNs loaded with GRV(1/2E + I), or MNs loaded with GRV(I). $*P < 0.05$ for administration with GRV(E + I)-loaded MNs compared with GRV(1/2E + I)-loaded MNs or GRV(I)-loaded MNs. (*D*) SEM image of GRV(E + I)-loaded MN after insertion for 4 h. (Scale bar: 200 μm.) (*E*) In vivo glucose tolerance test toward diabetic mice 1 h postadministration of GRV(E + I)-loaded MNs or insulin-loaded MNs in comparison to the healthy control mice. (*F*) Responsiveness was calculated based on the area under the curve (AUC) in 120 min, with the baseline set at the 0-min blood glucose reading. (*G*) Blood glucose changes of mice treated with additional administration of the MN-array patch 1 h postadministration of GRV(E + I)-loaded MNs. $*P < 0.05$ for additional administration with GRV(E + I)-loaded MNs compared with no additional administration. (*H*) Blood glucose changes of healthy mice administered an MN-array patch over time. (*I*) Quantification of the hypoglycemia index, which was calculated from the difference between the initial and nadir blood glucose readings divided by the time at which nadir was reached. $*P < 0.05$ for administration with GRV(E + I)-loaded MNs compared with insulin-loaded MNs. The black arrows indicate the administration points. Error bars indicate SD ($n = 5$).

enzymatic generation of gluconic acid. However, their effectiveness is limited by a slow response upon blood glucose changes, especially under a buffered physiological environment. This report demonstrates the first enzyme-based glucose-responsive insulin delivery strategy, to our knowledge, using sensitivity to hypoxia rather than pH variance. A local hypoxic microenvironment could be rapidly generated in PBS buffer solution due to the enzymatic consumption of oxygen, as evidenced by an oxygen-sensitive phosphorescent probe. Subsequently, the hydrophobic side-chains of HS-HA were reduced into hydrophilic chains, resulting in disassembly of GRVs, subsequently releasing insulin. The obvious change in morphology could be observed by TEM 20 min postincubation with PBS buffer containing 400 mg/dL glucose. The in vitro insulin release profile of GRVs indicated a remarkably faster release rate compared with the pH-sensitive–based formulations previously reported (19). In addition, the insulin release kinetics can be adjusted by varying the enzyme dose both in vitro and in vivo, further implying that the release of insulin undergoes a glucose-mediated and hypoxia-dependent process.

Furthermore, the GRVs were integrated into an HA-based MN-array patch for convenient, painless, and continuous administration of insulin. The cross-linked HA matrix not only

helped to improve mechanical strength and skin penetration capability but also restricted the loss of GRVs to avoid burst release. Additionally, the framework of both needle patches and vesicles was made from HA, which is highly biocompatible. The GRV(E + I)-loaded MNs exhibited excellent regulation of glucose into a normal range with fast responsiveness. Furthermore, in addition to the highly sensitive vesicles, the rapid uptake by the lymphatics through transcutaneous administration may contribute to the fast responsivity. The in vivo glucose tolerance test demonstrated not only that GRV-loaded MNs were responsive to glucose challenge but that they could also efficiently minimize the risk of hypoglycemia. In addition, the results of serial administration with MNs showed that it could precisely control glucose in a normal range for prolonged periods. Also considering that mice have reduced sensitivity to the human insulin used in this study, the real dose for potential human use will be significantly lower. This smart insulin patch with its novel trigger mechanism offers a clinical opportunity for closed-loop delivery of insulin in a fast glucose-responsive, pain-free, and safe manner. It will also guide the development of a useful drug delivery platform for treating other diseases using artificial vesicles, the behaviors of which can be "intelligently" activated and self-regulated by the variation of physiological signals.

Methods

Materials. All chemicals were purchased from Sigma–Aldrich unless otherwise specified and were used as received. Sodium HA (molecular mass of 300 kDa) was purchased from Freda Biochem Co., Ltd.. Human recombinant insulin (27.5 IU/mg of Zn salt) was purchased from Life Technology.

Preparation of GRVs. GRVs were prepared by self-assembly in aqueous solution. Briefly, 20 mg of amphiphilic HS-HA was dissolved in water/methanol (2:1 vol/vol), followed by addition of 10 mg of human insulin and 1.0 mg of GO_x. The emulsion was stirred at 4 °C for 2 h. Then, the methanol was removed by dialysis against deionized water for 1 d. The pH value of the resulting GRV suspension was adjusted to 5.3 (the pI of insulin) to remove the unloaded insulin by centrifugation at 6,200 × *g* for 10 min and further filtered by a centrifugal filter (100,000 Da molecular mass cutoff, Millipore) at pH 7.4. The final GRV suspension was stored at 4 °C for later study. The insulin loading capacity of GRVs was determined by measuring the loaded insulin content using a Coomassie Plus protein assay. The zeta-potential and size distribution were measured on the Zetasizer (Nano ZS; Malvern). The TEM images of GRVs were obtained on a JEOL 2000FX TEM instrument.

The animal study protocol was approved by the Institutional Animal Care and Use Committee at North Carolina State University and the University of North Carolina at Chapel Hill.

ACKNOWLEDGMENTS. We thank Dr. Elizabeth Loboa, Dr. Glenn Walker, Dr. Tushar K. Ghosh, and Xiaomeng Fang for providing experimental facilities and assistance in device characterizations. We acknowledge the use of the Analytical Instrumentation Facility at North Carolina State University, which is supported by the State of North Carolina and the National Science Foundation. This work was supported by Grants 1-14-JF-29 and 1-15-ACE-21 from the American Diabetes Association (to Z.G.) and by the North Carolina Translational and Clinical Sciences Institute, supported by the NIH Clinical and Translational Science Awards program (NIH Grant 1UL1TR001111) at the University of North Carolina at Chapel Hill.

1. Owens DR (2002) New horizons—Alternative routes for insulin therapy. *Nat Rev Drug Discov* 1(7):529–540.
2. Stumvoll M, Goldstein BJ, van Haeften TW (2005) Type 2 diabetes: Principles of pathogenesis and therapy. *Lancet* 365(9467):1333–1346.
3. Mo R, Jiang T, Di J, Tai W, Gu Z (2014) Emerging micro- and nanotechnology based synthetic approaches for insulin delivery. *Chem Soc Rev* 43(10):3595–3629.
4. Tabák AG, Herder C, Rathmann W, Brunner EJ, Kivimäki M (2012) Prediabetes: A high-risk state for diabetes development. *Lancet* 379(9833):2279–2290.
5. Owens DR, Zinman B, Bolli GB (2001) Insulins today and beyond. *Lancet* 358(9283): 739–746.
6. Bratlie KM, York RL, Invernale MA, Langer R, Anderson DG (2012) Materials for diabetes therapeutics. *Adv Healthc Mater* 1(3):267–284.
7. Ravaine V, Ancla C, Catargi B (2008) Chemically controlled closed-loop insulin delivery. *J Control Release* 132(1):2–11.
8. Veiseh O, Tang BC, Whitehead KA, Anderson DG, Langer R (2015) Managing diabetes with nanomedicine: Challenges and opportunities. *Nat Rev Drug Discov* 14(1):45–57.
9. Ohkubo Y, et al. (1995) Intensive insulin therapy prevents the progression of diabetic microvascular complications in Japanese patients with non-insulin-dependent diabetes mellitus: A randomized prospective 6-year study. *Diabetes Res Clin Pract* 28(2): 103–117.
10. Wu Q, Wang L, Yu H, Wang J, Chen Z (2011) Organization of glucose-responsive systems and their properties. *Chem Rev* 111(12):7855–7875.
11. Gordijo CR, et al. (2011) Nanotechnology-enabled closed loop insulin delivery device: In vitro and in vivo evaluation of glucose-regulated insulin release for diabetes control. *Adv Funct Mater* 21(1):73–82.
12. Gu Z, et al. (2013) Glucose-responsive microgels integrated with enzyme nanocapsules for closed-loop insulin delivery. *ACS Nano* 7(8):6758–6766.
13. Kataoka K, Miyazaki H, Bunya M, Okano T, Sakurai Y (1998) Totally synthetic polymer gels responding to external glucose concentration: Their preparation and application to on-off regulation of insulin release. *J Am Chem Soc* 120(48):12694–12695.
14. Gu Z, et al. (2013) Injectable nano-network for glucose-mediated insulin delivery. *ACS Nano* 7(5):4194–4201.
15. Chou DH, et al. (2015) Glucose-responsive insulin activity by covalent modification with aliphatic phenylboronic acid conjugates. *Proc Natl Acad Sci USA* 112(8):2401–2406.
16. Fischel-Ghodsian F, Brown L, Mathiowitz E, Brandenburg D, Langer R (1988) Enzymatically controlled drug delivery. *Proc Natl Acad Sci USA* 85(7):2403–2406.
17. Podual K, Doyle F, Peppas N (2000) Preparation and dynamic response of cationic copolymer hydrogels containing glucose oxidase. *Polymer (Guildf)* 41(11):3975–3983.
18. Podual K, Doyle FJ, 3rd, Peppas NA (2000) Glucose-sensitivity of glucose oxidase-containing cationic copolymer hydrogels having poly(ethylene glycol) grafts. *J Control Release* 67(1):9–17.
19. Tai W, et al. (2014) Bio-inspired synthetic nanovesicles for glucose-responsive release of insulin. *Biomacromolecules* 15(10):3495–3502.
20. Makino K, Mack EJ, Okano T, Kim SW (1990) A microcapsule self-regulating delivery system for insulin. *J Control Release* 12(3):235–239.
21. Aronoff S, Chen TC, Cheveldayoff M (1975) Complexation of D-glucose with borate. *Carbohydr Res* 40(2):299–309.
22. Kim SW, et al. (1990) Self-regulated glycosylated insulin delivery. *J Control Release* 11(1):193–201.
23. Tiegs G, Hentschel J, Wendel A (1992) A T cell-dependent experimental liver injury in mice inducible by concanavalin A. *J Clin Invest* 90(1):196–203.
24. Nunn A, Linder K, Strauss HW (1995) Nitroimidazoles and imaging hypoxia. *Eur J Nucl Med* 22(3):265–280.
25. Krohn KA, Link JM, Mason RP (2008) Molecular imaging of hypoxia. *J Nucl Med* 49 (Suppl 2):129S–148S.
26. Edwards DI (1993) Nitroimidazole drugs—Action and resistance mechanisms. I. Mechanisms of action. *J Antimicrob Chemother* 31(1):9–20.
27. Takasawa M, Moustafa RR, Baron J-C (2008) Applications of nitroimidazole in vivo hypoxia imaging in ischemic stroke. *Stroke* 39(5):1629–1637.
28. Chauhan VP, et al. (2013) Angiotensin inhibition enhances drug delivery and potentiates chemotherapy by decompressing tumour blood vessels. *Nat Commun* 4:2516.
29. Khetan S, et al. (2013) Degradation-mediated cellular traction directs stem cell fate in covalently crosslinked three-dimensional hydrogels. *Nat Mater* 12(5):458–465.
30. Mo R, Jiang T, DiSanto R, Tai W, Gu Z (2014) ATP-triggered anticancer drug delivery. *Nat Commun* 5:3364.
31. Martanto W, et al. (2004) Transdermal delivery of insulin using microneedles in vivo. *Pharm Res* 21(6):947–952.
32. Prausnitz MR, Langer R (2008) Transdermal drug delivery. *Nat Biotechnol* 26(11): 1261–1268.
33. Yang SY, et al. (2013) A bio-inspired swellable microneedle adhesive for mechanical interlocking with tissue. *Nat Commun* 4:1702.
34. DeMuth PC, et al. (2013) Polymer multilayer tattooing for enhanced DNA vaccination. *Nat Mater* 12(4):367–376.
35. Heo YJ, Shibata H, Okitsu T, Kawanishi T, Takeuchi S (2011) Long-term in vivo glucose monitoring using fluorescent hydrogel fibers. *Proc Natl Acad Sci USA* 108(33):13399–13403.
36. Harvey AJ, et al. (2011) Microneedle-based intradermal delivery enables rapid lymphatic uptake and distribution of protein drugs. *Pharm Res* 28(1):107–116.
37. Chung JE, et al. (2014) Self-assembled micellar nanocomplexes comprising green tea catechin derivatives and protein drugs for cancer therapy. *Nat Nanotechnol* 9(11): 907–912.
38. Yu H, Qiu X, Nunes SP, Peinemann K-V (2014) Biomimetic block copolymer particles with gated nanopores and ultrahigh protein sorption capacity. *Nat Commun* 5:4110.
39. Will Y, Hynes J, Ogurtsov VI, Papkovsky DB (2006) Analysis of mitochondrial function using phosphorescent oxygen-sensitive probes. *Nat Protoc* 1(6):2563–2572.
40. Fercher A, Borisov SM, Zhdanov AV, Klimant I, Papkovsky DB (2011) Intracellular O_2 sensing probe based on cell-penetrating phosphorescent nanoparticles. *ACS Nano* 5(7):5499–5508.
41. Seki Y, Nakamura T, Okami Y (1970) Accumulation of 2-aminoimidazole by Streptomyces eurocidicus. *J Biochem* 67(3):389–396.
42. Prausnitz MR (2004) Microneedles for transdermal drug delivery. *Adv Drug Deliv Rev* 56(5):581–587.
43. Fletcher JE (1980) On facilitated oxygen diffusion in muscle tissues. *Biophys J* 29(3): 437–458.
44. Michaels A, Chandrasekaran S, Shaw J (1975) Drug permeation through human skin: Theory and in vitro experimental measurement. *AIChE J* 21(5):985–996.
45. Dowd GS, Linge K, Bentley G (1983) Measurement of transcutaneous oxygen pressure in normal and ischaemic skin. *J Bone Joint Surg Br* 65(1):79–83.